Time-of-flight modulated intensity small-angle neutron scattering measurement of the self-diffusion constant of water

Kuhn, Stephen J.; Geerits, Niels; Franz, Christian; Plomp, Jeroen; Dalgliesh, Robert M.; Parnell, Steven R.

DOI
10.1107/S1600576721002612

Publication date
2021

Document Version
Accepted author manuscript

Published in
Journal of Applied Crystallography

Time-of-Flight MI-SANS measurement of the self-diffusion constant of water

Stephen J. Kuhn,[a,*] Niels Geerits,[b,*] Christian Franz,[c,d] Jeroen Plomp,[e] Robert M. Dalgliesh[f] and Steven R. Parnell[e]

[a] *Center for Exploration of Energy and Matter, Indiana University, Bloomington, 47408, USA,* [b] *Atominstitut, TU Wien, Stadionallee 2, 1020 Vienna, Austria,* [c] *Physik Department, Technische Universität München, Garching D-85748, Germany,* [d] *Heinz Maier-Leibnitz Zentrum (MLZ), Technische Universität München, Garching D-85748, Germany,* [e] *Faculty of Applied Sciences, Delft University of Technology, Mekelweg 15, 2629 JB Delft, The Netherlands, and* [f] *ISIS, Rutherford Appleton Laboratory, Chilton, Oxfordshire, OX11 0QX, UK*

Neutron spin echo; SANS; Water

Abstract

The Modulated Intensity by Zero Effort-Small Angle Neutron Scattering (MI-SANS) technique is used to measure scattering with a high energy resolution on samples normally ill-suited for neutron resonance spin echo. Here we measure the self-diffusion constant of water over a q-t range of 0.01-0.2 Å^{-1} and 70-500 picoseconds. In addition to demonstrating the methodology of using time-of-flight MI-SANS instruments to observe diffusion in liquids, our result supports previous measurements on water performed with different methods. This polarized neutron technique simultaneously

measures the intermediate scattering function for a wide range of time and length scales. Two RF flippers were used in a spin echo set-up with a 100 kHz frequency difference in order to create a high resolution time measurement. We compare our results to self-diffusion measurements made by other techniques as well as the general applicability of MI-SANS at a time-of-flight source.

1. Introduction

The dynamics of liquid systems is a complex field where many mechanisms influence the behavior. In water (H_2O) and other liquids, short time-scale dynamics are determined by molecular rotations and vibrations, while long time-scale dynamics are dominated by self-diffusion. These dynamics are characterized by the intermediate scattering function, $S(q, \tau)$, which is a distribution function containing information on the length and time scales of the sample dynamics (Mezei, 2003) such as the self-diffusion constant, D, which is defined by the stochastic motion of molecules at thermal equilibrium (Price 2009).

There are several methods for determining the diffusion constant. Molecular dynamics (MD) simulations can compute the intermediate scattering function and diffusion constant, which can be compared to experiments. Nuclear Magnetic Resonance (NMR) is an experimental probe of the diffusion constant using gradient echo methods. However, NMR does not give information about the reciprocal space dependence (Price 2009). Scattering methods have long been applied to the investigation of water diffusion, for comprehensive reviews the reader is directed to Price 2009, Amann-Winkel et al. 2016 and Holz et al. 2000.

In this paper, we present the methodology of using a high resolution neutron scattering technique to measure the intermediate scattering function and diffusion constant and apply it to the important case of bulk water at ~ 300 K. The Modulated Intensity

by zero effort-Small Angle Neutron Scattering (MI-SANS also called MIEZE-SANS) technique is a variant of neutron (resonance) spin echo (Mezei, 1972) (NSE/NRSE) (Golub and Gähler 1987, Gähler et al., 1992: Hank et al. 1997). Both are very high resolution neutron scattering measurements of dynamics in the ps to ns time regime (Franz et al. 2019b; Lebedev et al. 1999; Bleuel et al. 2006). The basis of MI-SANS is that two radio frequency (RF) flippers are used to create a high frequency, but resolvable, time oscillation in a neutron signal that is scattered by a sample. MI-SANS is complementary to NRSE and offers several distinct advantages. Most notable for this experiment are that it only requires two RF flippers (as opposed to four in NRSE), leading to an easier instrument set-up than traditional NRSE, and that all of the spin manipulations are performed before the sample, so depolarizing samples and sample environments do not impede the measurement. For this experiment on water (H_2O), the incoherent neutron scattering from hydrogen would reduce the maximum polarization on a conventional NSE instrument to 1/3. In MI-SANS, because the polarization does not need to be maintained through the sample, the incoherent scattering simply creates a larger signal at the detector. This is the case for any hydrogenous system and the in-sensitivities to depolarization also simplifies the use of sample environments with high magnetic fields.

We have set-up the MI-SANS instrument on a time-of-flight beamline with two RF flippers performing $\pi/2$ flips with a resulting 100 kHz frequency difference, a ^{3}He analyzer, and a standard ^{3}He tube detector array. Time-of-flight MI-SANS measures the intermediate scattering function for a range of scattering angles and wavelengths simultaneously. The instrument was tuned to measure $S(q,\tau)$ at time scales of $\sim 50-500$ ps and scattering vectors ranging from $\sim 0.02-0.07$ Å^{-1}, in the domain dominated by self-diffusion for water. We demonstrate the effectiveness of using a time-of-flight MI-SANS instrument for studying liquid dynamics. Additionally, we find a

bulk diffusion constant for water of $2.45 \pm 0.32 \times 10^{-9}\mathrm{m}^2/\mathrm{s}$, in good agreement with the NMR literature and which sets a standard for comparison of constrained water samples.

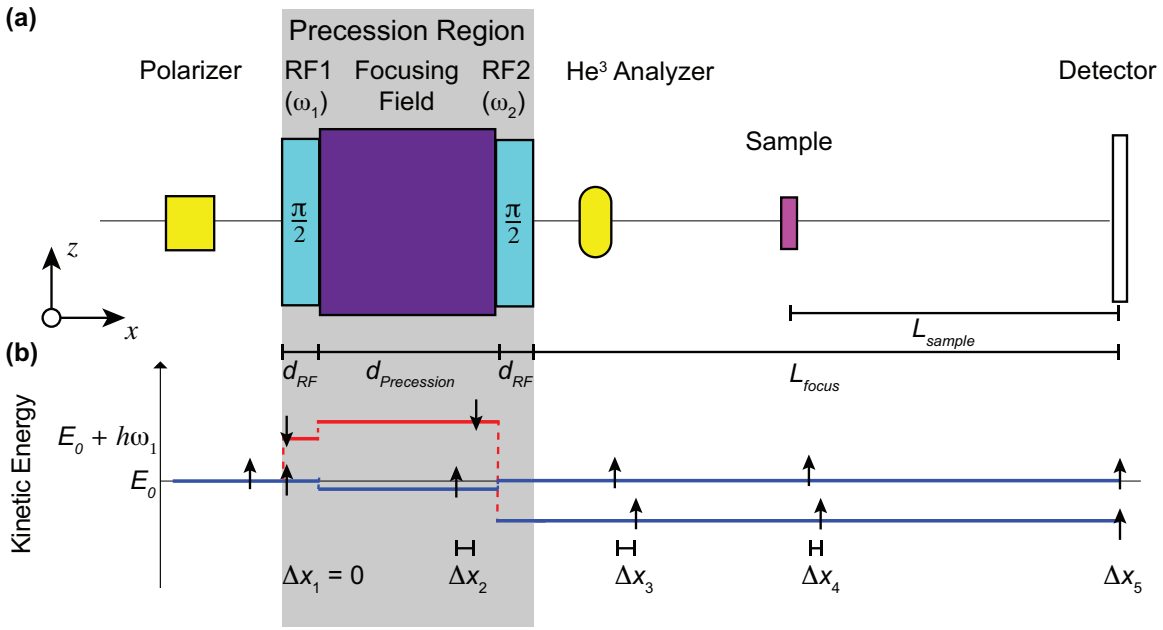

Fig. 1. Instrument set-up and separation of the neutron states. (a) A side view of the magnetic components of the MI-SANS instrument are shown. The beam travels in the x direction through the polarizer, RF Flipper 1 (with angular frequency ω_1), the focusing field (a static, $z-$direction, guide field of length d_{Prec}), and RF Flipper 2 (with frequency $\omega_2 > \omega_1$). Both RF flippers are of length d_{RF} and set to perform $\pi/2$ spin flips, which creates a superposition of up and down spin states. The beam passes through a ^{3}He analyzer which absorbs the spin down neutron states. The neutron then scatters from the sample and is measured by the 2-dimensional detector, which is placed L_{focus} away from RF2 and L_{sample} away from the sample. (b) The kinetic energy and separation of the spin states is shown along the instrument. The beam is initially polarized in the $z-$direction. The $\pi/2$ flip in RF1 creates a superposition of the up and down spin states, with the flipped spin state gaining an energy of $\hbar\omega_1$ from the flipper. In the focusing field, the spin states kinetic energy is lowered/raised by the Zeeman term. The difference in kinetic energy creates a spatial separation, as shown by Δx_2. RF2 is set to a larger frequency (ω_2) and hence will cause a larger change in energy of the flipped neutron spin. RF2 also creates a superposition of up and down states for the two states entering it, but the ^{3}He analyzer is set to filter the down state, leaving two different spatially separated (Δx_3), energy states with the same spin. Because the kinetic energy is different, the spatial separation decreases as the states continue along the beamline. The two energy states pass through the sample with separation Δx_4 before reaching the detector with separation Δx_5.

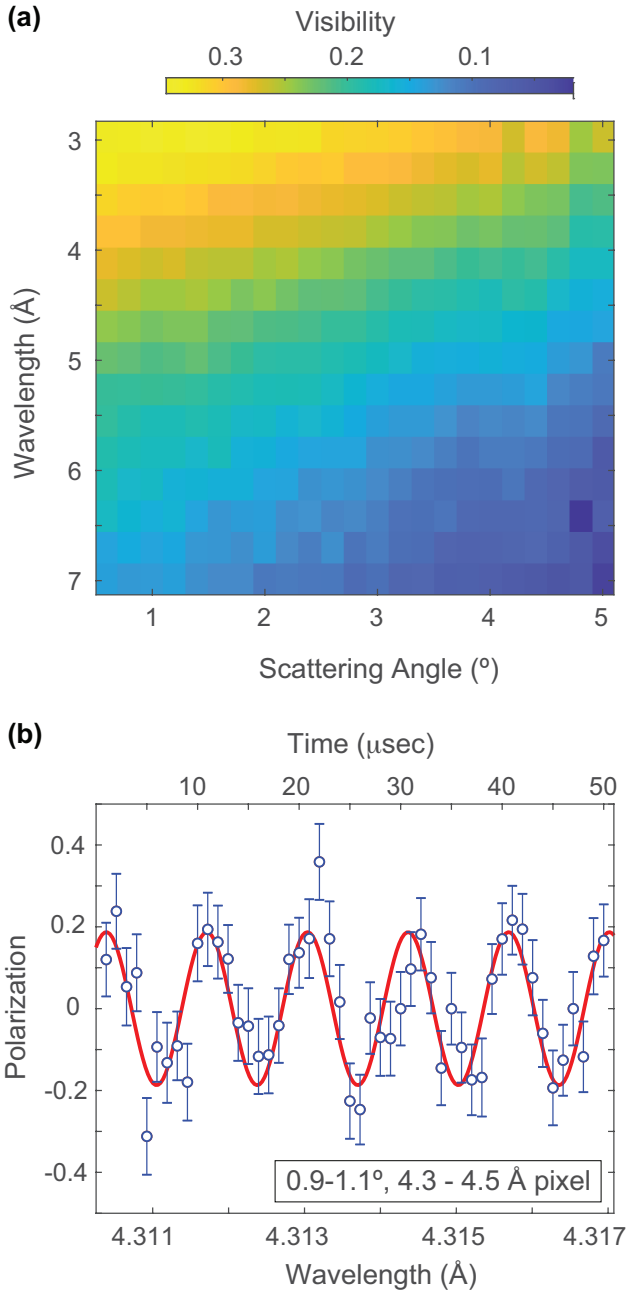

Fig. 2. (a) The visibility of glassy carbon vs. angle and wavelength. (b) The polarization vs. wavelength for part of a single pixel of scattering angle 0.9-1.1°. On the Larmor time-of-flight instrument, wavelength corresponds to the detector measurement time (top x-axis). Error bars represent the statistical counting error. The modulation is fitted using a cosine function (red curve) to find the visibility. The period is 10 μs, as expected from the 100 kHz MI-SANS frequency.

2. Methods

The experiment was conducted on the Larmor instrument at the ISIS pulsed neutron and muon source (ISIS DOI# 10.5286/ISIS.E.RB1920600). The instrument configuration is shown schematically in Fig. 1. The incident beam polarization is selected to be in the + or − z direction using a polarizer consisting of a v-cavity and a gradient RF flipper (not shown). The neutron precesses in a region with two RF Flippers, RF1 and RF2. Before the sample is a spin polarized ^{3}He cell in a magnetostatic cavity for polarization analysis. The polarizer, flippers, and analyzer are in a vertical guide field (focusing field) of 8 gauss to maintain the neutron polarization. The beam stays within evacuated flight tubes with the exception of a $\sim$ 1 m region in the sample and ^{3}He analyzer area. Collimation is achieved with a 15 mm pinhole at the sample position and a 25 mm x 25 mm aperture located approximately 5 m before the sample position.

The longitudinal RF flippers RF1 and RF2 consist of a vertical (z-direction) static field and a horizontal RF field. The static field strength is tuned to $B_{1(2)} = \omega_{1(2)}/\gamma$, where $B_{1(2)}$ is the resonance field for RF1 (RF2), $\omega_{1(2)}$ is the RF frequency, and γ is the neutron gyromagnetic ratio. The flippers were separated by 1.57 m and run in $1/t, \pi/2$ mode, meaning that the RF field strength is ramped to produce a $\pi/2$ spin flip for each neutron wavelength, λ, similar to the set-ups by Zhao et al. (Zhao et al., 2015) and Brandl et al. (Brandl et al., 2012).

The RF flippers in this experiment were tuned to $\pi/2$ mode in order to simplify the set-up of the instrument. In a traditional MI-SANS experiment, the RF flippers perform a π flip meaning that the initial and final neutron polarization direction must be re-oriented with a v-coil (Geerits et al. 2019). In $\pi/2$ mode, the v-coil is not required which saves approximately 1 day of set-up time but reduces the accessible Fourier time by a factor of two.

Calibration of $1/t, \pi/2$ mode is performed one flipper at a time. The first step is the tuning of the static field of the flipper, which is accomplished by measuring the beam polarization while scanning the static field in small ($\approx 0.2G$) increments. This field is very sensitive to detuning since the RF coils are quite long. In this step the RF coil is driven using a constant amplitude sinusoidal waveform (continuous waveform CW). The beam polarization can be described as a sine function in this mode. At the optimal static field setting the amplitude of this function is maximal. Once the static field is calibrated, the $1/t$ envelope is calculated using the wavelength at which the first π flip occurs in CW mode and the flipper to source separation. Next the beam polarization is measured with $1/t$ ramping to confirm all wavelengths are being flipped. Finally the flipper is switched from π flip mode to $\pi/2$ mode, by halving the current in the RF coil. This current is monitored using a pickup coil which is part of a feedback loop controlling the RF amplifier gain setting. Whether the flipper has been adequately tuned to $\pi/2$ mode can be gauged by measuring the beam polarization, which should be zero for all wavelengths. Once the tune has been confirmed, the RF coil can be switched off, so that the second flipper can be tuned. After tuning both flippers both RF coils can be switched back on to begin $\pi/2$ MIEZE measurements. In $\pi/2$ MIEZE the magnetic precession region begins at the first RF flipper, tuned to 533.4 kHz and ends at the second RF flipper tuned to 633.4 kHz, producing a frequency difference of 100 kHz.

The MI-SANS focusing condition can be explained as the spatial recombining of two neutron spin states with different group velocities. In the $\pi/2$ MI-SANS set-up, the incoming neutrons are polarized in the z-direction before entering RF1. RF1 is calibrated to perform a $\pi/2$ flip of the neutrons. This yields a superposition of 2 neutron spin states in the $\pm$ z direction with different energies. The difference in energies corresponds to a difference in velocities and hence a longitudinal spatial

separation between the two spin states. RF2 is set to a higher frequency than RF1, leading to the neutron spin state that was spatially behind having a larger energy (higher velocity) than the spin state that was spatially ahead, as depicted in Fig. 1(b). This difference in energies persists through the ^{3}He analyzer, which filters spins in the negative z direction. Thus, after the analyzer, there are two spatially separated neutron states with the same spin direction but different velocities. The relative velocity after the flipper is tuned so that the states will overlap at the desired focal length L_{focus}, where the detector is placed:

$$L_{focus} = \frac{\omega_1 d_{Prec} - \int_0^{d_{Prec}} \omega_{FF}(x)dx}{\Delta\omega} + d_{RF} \tag{1}$$

Here d_{RF} is the RF flipper length, d_{Prec} is the separation between the two RF flippers, ω_1 is the frequency of the first RF flipper, $\Delta\omega = \omega_2 - \omega_1$ the difference in the RF flipper frequency, and $\omega_{FF} \approx \gamma B_{FF}$, where B_{FF} is the focusing field strength. This term will also include any stray field from the RF flippers (Geerits et al., 2019). When the detector is placed at L_{focus}, it will measure an oscillating intensity due to the interference between the energy states (Keller et al. 2002). Thus the signal can be interpreted as coming from the self-interference of single neutrons. This is evidenced by the fact that the spin-echo group can be described using the longitudinal autocorrelation of the wavefunction (Golub 1992). Naturally if the beam contains neutrons described by different wavepackets the spin echo group is given by the sum of all possible wavepacket autocorrelations.

In the case of the RF flippers being in $\pi/2$ mode, the difference frequency is the same as the MI-SANS frequency (Keller et al. 2002; Zhao et al. 2015). In this experiment, the approximately 8 Gauss guide field also served as the focusing field, B_{ff}, between the RF flippers (Jochem et al., 2020). The setup is designed in such a way that the flippers are always situated in a guide field, hence the range of focusing field values are limited by the constraint that we must not reduce the guide field to a point where

the beam depolarizes.

The spatial separation of the neutron spin states is represented in Fig. 1(b) by Δx. At the entrance of RF1 (Δx_1), the neutron spin states are split into up and down with different kinetic energies, but there is not yet any spatial separation. Before RF2 (Δx_2), the higher kinetic energy spin state has moved spatially in front of the lower kinetic energy state. Because of the spin flip in RF2, after the ^{3}He analyzer (Δx_3), the spin state with the higher kinetic energy is behind the other state. When the states pass through the sample (Δx_4), they have moved closer together than Δx_3. The focus length, L_{focus}, is tuned so that, if there is no sample in the beam, the states will exactly recombine at the detector as there is no spatial separation ($\Delta x_5 = 0$). The spatial separation can be related to the time separation by $\Delta t \approx \Delta x * h/(2 * \lambda * E_0)$, where E_0 is the neutron energy.

A ^{3}He analyzer acts as a neutron spin filter to allow through neutrons polarized in the z-direction. The efficiency is wavelength-dependent, characterization of this was performed using transmission measurements (Boag et al., 2007). This gave a ^{3}He polarization of 65-70% on each cell change. The ^{3}He cell used was a double silicon window cell with quartz body, the single crystal silicon windows were chosen to eliminate the small angle scattering that occurs with glass cells (Babcock et al. 2013). The cell is 10cm long along the beam direction, was pressurized to 1 bar and had an on beam lifetime (exponential decay constant (T_1)) of ∼100 hours. The cell was mounted in a magnetostatic cavity similar to the one described in (Parnell et al. 2009) and monitored using an FID NMR system similar to that described in (Parnell et al. 2008), the cell was changed each day to maintain a high polarization. The resulting analyzer power was ≈90% across the neutron wavelength band used.

The samples were a 1 mm thick cell of deionized water (H_2O) and a glassy carbon standard (Cappelletti 2018). Measurements were alternated between the water and

the standard to correct for the time dependent decay of the ^{3}He polarizer. The water sample was measured at $\sim$ 300 K, which was kept constant by water bath cooling. The beam size was defined by a 15 mm circular aperture, which gave a detected intensity of 200 neutrons per second. Data was recorded in event-mode by a 60 x 60 cm ^{3}He tube array with 0.4 x 0.8 cm pixel size, that was placed 4.45 m from the sample position and 6.45 m from the second RF flipper. Each tube has a thickness of 0.8 cm. The timing resolution of the data acquisition electronics was set to 1 microsecond. Though we note that the effective time resolution also depends on the tube diameter, neutron wavelength and filling pressure. Using Monte Carlo simulations we estimated the expected visibility at various wavelengths. The lower time resolution leads to a simple reduction factor in the visibility, which can be removed through normalization. A discussion of the detector optimization is included below. A beamstop masked the direct beam in order to reduce the background signal, leading to a measurable angle range of 0.7° to 5.5°.

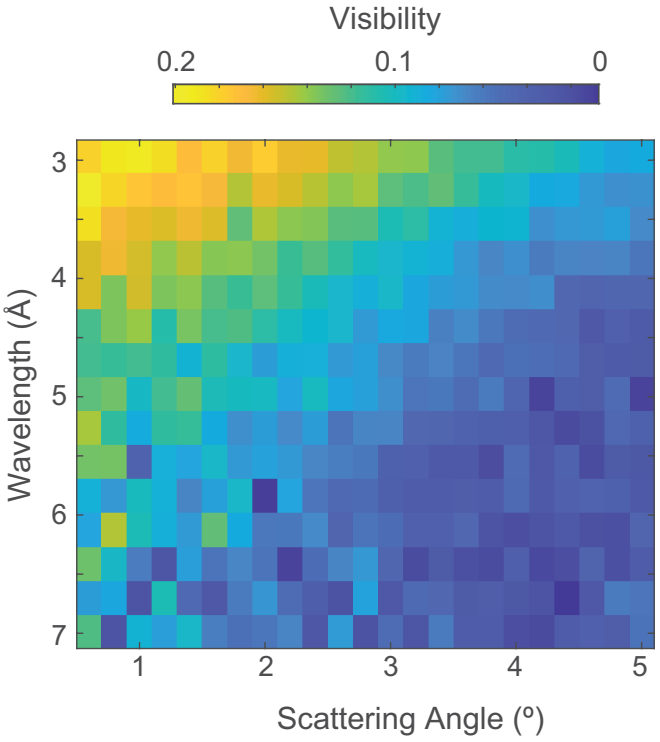

Fig. 3. The visibility of water vs. angle and wavelength. For each pixel, the modulation amplitude is fitted by a cosine function to get the visibility, after correcting by the ^{3}He analyzer efficiency and air scattering background using Eqn. 2.

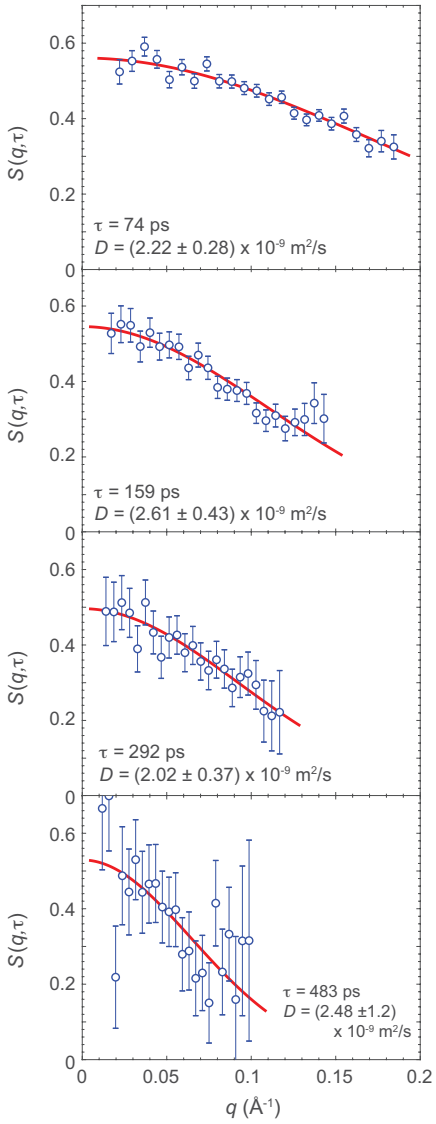

Fig. 4. $S(q,\tau)$ values plotted at four Fourier times, τ. Each τ corresponds to a specific wavelength of 2.95 Å, 3.85 Å, 4.65 Å, and 5.55 Å, respectively, with 0.3 Å bins. Error bars correspond to the MI-SANS visibility fit uncertainty from each pixel. The diffusion constant, D, is fitted from $S(q,\tau)$ using Eqn. 8.

3. Results

Time dependent MI-SANS scattering was measured for solid glassy carbon (which acts as a standard) and for water. The glassy carbon data is useful both as a known standard to prove the functionality of MI-SANS and as a way for measuring the

instrument resolution function for normalization due to its scattering being purely elastic. The water data can be reduced to obtain the diffusion constant, D.

MI-SANS characterizes a sample by the measurement of the visibility. The visibility (also called the contrast) is defined as the intensity difference between the two polarization states divided by their sum: $V = (I_+ - I_-)/(I_+ + I_-)$, where I_+ and I_- are the intensity of the initially up (positive z) and down (negative z) polarized beam, respectively. MI-SANS measures the visibility for a range of wavelengths and scattering angles. The visibility of the glassy carbon is shown in Fig. 2(a). At large angles statistics are low due to only the corners of the detector being used. On the detector, the visibility V is measured with time binning set to 1 μs and an angular binning of 0.2°. This angular binning corresponds to the highest angular resolution with sufficient statistics to obtain good fits. Each pixel within Fig. 2(a) contains 2000 of these time bins. The visibility of each pixel is determined by fitting the amplitude of the time-oscillating polarization signal to a cosine function.

Figure 2(b) shows a subset of the pixel at 0.9-1.1°, 4.3-4.5 Å and the cosine fit used to determine the visibility. The wavelength directly corresponds to the detector time. For clarity, only a portion of the time bins in the pixel are shown. The visibility of the glassy carbon is not corrected for the ^{3}He analyzer transmission and background counts were found to be negligible compared to the signal.

The glassy carbon scattering does not contain any dynamics. Furthermore the background to signal ratio is sufficiently small such that the background can be ignored. Therefore the visibility is fully determined by the reduction factor and instrument limitations (Martin 2018). However, self-diffusion of the water sample causes a Fourier time-dependent shift to the scattering, as the scattering amplitude is dependent on the energy transfer between sample and beam. This is an inherent characteristic of water that we measure with MI-SANS.

The visibility of the MI-SANS signal from water, Fig. 3, is determined by the same procedure as for the glassy carbon, except the data is background subtracted to account for a higher relative background rate. The background is corrected by including an extra term in the visibility definition, $V_{BG} = \frac{I_+ - I_-}{I_+ + I_- + 2I_{BG}}$. This assumes the background is from air and other parasitic scattering along the beamline, leading to an unpolarized background that is the same for I_+ and I_- and thus cancels on the numerator.

A correction matrix, α, is defined for the background at each pixel.

$$V_{BG} = \frac{I_+ - I_-}{(I_+ + I_-)[1+\alpha]} = \frac{V}{1+\alpha} \tag{2}$$

The α correction matrix is found using the background data taken with the sample removed from the beam. The I_+ and I_- background data are binned in the same manner as the water data. Because only the sum of I_+ and I_- is needed, all 2000 time bins are summed to increase statistics. To determine the background corrected visibility, each visibility pixel is multiplied by the corresponding $1+\alpha$ value.

The MI-SANS results can be directly converted into the more conventional neutron scattering parameters of scattering vector q and time τ. In the case of elastic scattering where the energy transfer is negligible the q value is determined by the scattering angle and the wavelength: $q_e = 4\pi \sin(\theta/2)/\lambda$. For quasi elastic scattering a first order correction must be applied $q_{qe} = q_e + \Delta q$, which takes the energy transfer into account. It can be shown that $\Delta q = \pm \frac{m\omega}{\hbar k} sin(\frac{\theta}{2})$, with $\hbar\omega$ the scattering energy and k the initial wavevector. In this experiment the first order correction amounts to only $1-2\%$ at most and is therefore neglected. In this experiment, q is assumed to be radially isotropic. At small scattering angles, $\sin(\theta/2) \approx \theta/2$ and several points are at equivalent q in Fig. 2(a) and Fig. 3. The Fourier time, τ, is defined as the neutron phase shift over the angular frequency $\tau = \Delta\phi/\Omega$,with Ω the neutron angular frequency. The phase

shift can also be written in terms of the instrument parameters $\Delta\phi = \Delta\omega t$, where t is the time the neutron travels between the sample and the detector. The Fourier time can be written in terms of L_{sample} with:

$$\tau = \frac{\Delta\omega m_n^2 \lambda^3}{2\pi h^2} L_{sample}, \tag{3}$$

here m_n is the neutron mass (Franz et al., 2019b, Keller et al., 2002).

The ratio of the visibility of the water sample and glassy carbon sample yields the intermediate scattering function, $S(q,\tau) = \frac{V_{water}(q,\tau)}{V_{carbon}(q,\tau)}$ of water. In this τ-q domain the dynamics in water are dominated by self-diffusion, while other inelastic processes such as vibrations and rotations of the molecules can be ignored. The position of a water molecule can therefore be modeled using the diffusion equation

$$\frac{\partial}{\partial\tau} G(r,\tau) = D\nabla^2 G(r,\tau) G(r,0) = \delta(r-r') \quad \lim_{r\to\infty} G(r,\tau) = 0 \tag{4}$$

where D is the self diffusion coefficient and $G(r,\tau)$ is the van Hove correlation function, describing the probability of finding a water molecule at position r and time τ. We assume that at $\tau = 0$ the position of the molecule was well defined at $r = r'$. The solution is simply a Gaussian function,

$$G(r,r,'\tau) = \frac{1}{\sqrt{4\pi D\tau}} e^{-\frac{(r-r')^2}{4D\tau}}. \tag{5}$$

This function models the probability density of finding a water molecule at position r and time τ, given that at $\tau = 0$ the particle was located at $r = r'$. To determine the intermediate scattering function we must calculate the Fourier transform of $G(r,\tau)$ with respect to r.

$$S(q,r',\tau) = c\int G(r,r',\tau) e^{-iqr} dr = a e^{-iqr'} e^{-Dq^2\tau} \tag{6}$$

The amplitude factor a models the fast dynamics at low τ, which are not taken into account by diffusion. The visibility can be obtained by averaging in r' over the sample

volume, $\mathcal{D}$.

$$V = RS_{\mathcal{D}}(q,\tau) = aRe^{-Dq^2\tau}\int_{\mathcal{D}} e^{-iqr'}dr' \tag{7}$$

with R the reduction factor due to various factors pertaining to instrument resolution (i.e. timing resolution). To remove contributions from the instrument resolution we normalize $S_{\mathcal{D}}(q,\tau)$, by the intermediate scattering function of a static sample (i.e. the glassy carbon). Ideally, the position of the atoms in this sample can be described by $G(r,r',\tau) = \delta(r-r')$. The Fourier transform e^{-iqr}, yields the visibility for this ideal sample: $V_0 = \int_{\mathcal{D}} e^{-iqr'}dr'$. The intermediate scattering function can therefore be derived as:

$$S(q,\tau) = \frac{V(q,\tau)}{V_0(q,\tau)} = ae^{-Dq^2\tau} \tag{8}$$

In this MI-SANS experiment, the intermediate scattering function is given by the ratio between the water and glassy carbon visibilities. $S(q,\tau)$ is plotted for several Fourier times in Fig. 4. Each Fourier time is effectively a normalized horizontal slice in the visibility plot, Fig. 3. However, the q-range measured for each τ is different, with higher τ having a smaller range. The data at each τ are fit by Eqn. 8.

The diffusion constants extracted for each Fourier time are shown in Fig. 5. The average value, shown by the red line, is $2.45 \pm 0.32\times 10^{-9}\mathrm{m}^2/\mathrm{s}$, which is within the error bars for each Fourier time, so no trend is seen.

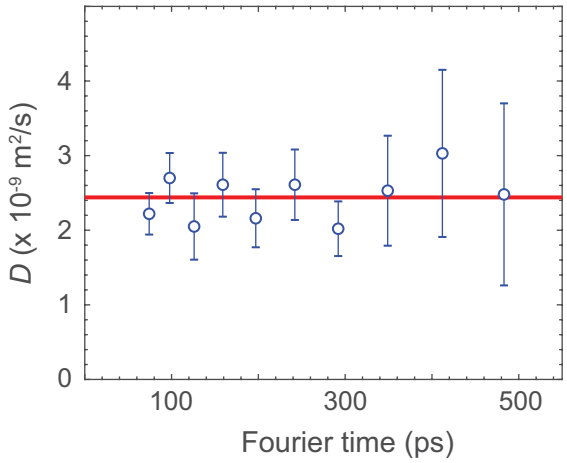

Fig. 5. Diffusion constants for water extracted from the fit of $S(q,\tau)$ for each Fourier time, τ. The average value of $2.4\times\ 10^{-9}\mathrm{m}^2/\mathrm{s}$ is shown by the red line. Error bars correspond to the 70% confidence region of the fit.

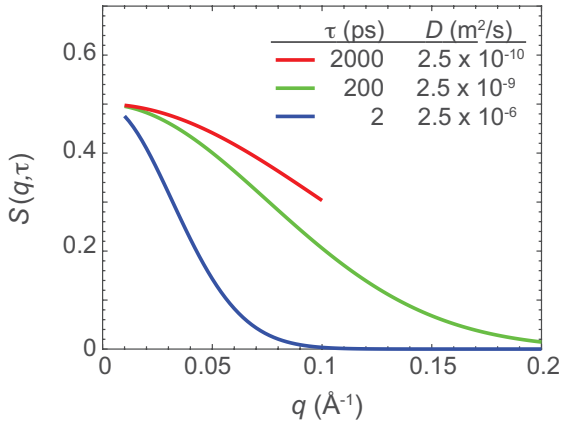

Fig. 6. The range of diffusion constants that can be measured with the MI-SANS technique at the Larmor instrument. The lines represent the maximum (blue), minimum (red), and water (green) intermediate scattering functions on the Larmor instrument set to the appropriate Fourier time, τ.

4. Discussion

Our results expand upon the previous measurements of the dynamics of water at ambient temperature obtained by neutron scattering and NMR. Previous Quasi-elastic

Neutron Scattering (QENS) measurements considering water diffusion used a random jump diffusion model, which applies well to the small q values used in this experiment, but also to larger q (Teixeira et al. 1985; Cavatorta et al. 1994; Egelstaff et al. 1967). A diffusion constant of $2.36\times\ 10^{-9}\mathrm{m}^2/\mathrm{s}$ was found (Cavatorta et al. 1994).

NMR is frequently used to measure diffusion in liquids and several measurements have been made on water. There is a wide range of diffusion constant values that can be measured with NMR. NMR relaxometry useful for slower materials (D down to 10^{-9} m^2/s) (Kruk 2012) and NMR pulsed gradient field methods useful for the range of 10^{-6} - $10^{-14}\mathrm{m}^2/\mathrm{s}$ (Price 2009). NMR results of water at $\sim$ 300 K have generally shown values around $2.3\ \times\ 10^{-9}\mathrm{m}^2/\mathrm{s}$, within the error bars of the MI-SANS results (Trappeniers et al. 1965, Wiengartner 1982). One difference between MI-SANS and NMR is that MI-SANS does not need to apply a magnetic field to the samples, so samples that induce stray fields can be studied without extra corrections.

Another purpose of this experiment was to compare our MI-SANS measurement on a time-of-flight source with measurements performed at a constant wavelength source. The implementation of MI-SANS geometry has been proposed on a time-of-flight source (Bleuel et al. 2005; Bleuel et al. 2006) and demonstrated using a reactor source with a chopper on a skyrmion system (Brandl et al. 2012). The RESEDA beamline at FRM-II neutron source has performed many MI-SANS experiments at constant wavelength (Franz et. al. 2019b). The direct advantages of the constant wavelength source are an easier determination of the q value at various points on the detector and, usually, an overall higher neutron flux. However, the time-of-flight source can use the modulation in the wavelength spread as a way to tune the L_{focus} length (Geerits et al. 2019). Additionally, the detector simultaneously measures a wide range of Fourier times and q-ranges, leading to an efficient use of the different neutron wavelengths. We measured q-scans for ten Fourier times, despite the relatively low scattering from

the water sample. This also means that the MI-SANS time can be changed without re-tuning the RF flippers. The time-of-flight source still offers some flexibility in regards to acquiring sufficient statistics because the wavelength/ time bins can be rescaled to include more modulations, leading to lower error in the fit (in our case, each bin included 2000 points). Although ultimately the constant wavelength source will have the maximum flexibility of choosing each Fourier time measured.

The MI-SANS technique can be applied to many other materials to measure the intermediate scattering function and self-diffusion. Materials with diffusion ten times slower or 100 times faster than water could both be fit with MI-SANS at Larmor, as shown by the expected curve for those materials in Fig. 6. The listed Fourier times can be achieved by adjusting $\Delta\omega$ within its tolerance at Larmor. The q range could be expanded even more by adjusting the detector position in the y direction and, with careful set-up, the $\Delta\omega$ could be even larger. MI-SANS is especially useful in hydrogenous materials, where conventional neutron spin echo has limited polarization (Franz et al., 2019b). Another useful feature is that it can accept a wide variety of sample environments, including strong magnetic fields (Kindervater et al., 2015). One application we foresee is measuring the diffusion of liquid neutron moderators. Their design depends on a good understanding of their diffusion and they are often hydrogenous (Iverson et al., 2018).

As well as selecting a time-of-flight or constant wavelength source, there are also multiple options in choosing what type of neutron analyzer to use. In this experiment a ^{3}He analyzer was used instead of a supermirror. The ^{3}He cell has less background scattering at low q than supermirrors but decreases the overall polarization. Additionally, the ^{3}He cell's neutron transmission varies significantly across neutron wavelengths and the cell must be repolarized several times throughout the average experiment (Boag et al., 2009; Parnell et al., 2015; Salhi et al., 2019).

We have implemented this technique on an existing polarized SANS instrument using the coils which were developed for Larmor labelling (Geerits et al., 2019), despite the good agreement of the diffusion constant with other measurements there are several areas of improvement remaining. First, the detector causes a significant loss in the intensity modulation signal, as the tubes are 0.8 cm diameter. This reduces the effective timing resolution of the detector as the neutron velocity decreases. Using measurements of detector transmission and Monte-Carlo modelling of neutron absorption in the detector we calculated a maximum visibility of 54% at 3 Å that drops to $\sim 20\%$ at 5 Å. This visibility reduction is solely caused by the detector. Visibility can be improved by utilizing a Cascade detector with a Gas Electron Multiplier (GEM) with a much thinner active area (Köhli et. al 2016). Improvements to the ^{3}He polarization of 60-70% in our setup are also possible with 88+% now being achieved (Chen et al. 2014). It is also possible to remove the time dependence by online pumping (Boag et al., 2009; Parnell et al., 2015; Salhi et al., 2019) . Further gains in flux at the sample position are also possible by utilizing guides before the sample, however this is a compromise between flux and q-range as this will transport more neutron divergence.

5. Conclusion

We have shown that the MI-SANS technique can be simply applied to measure the intermediate scattering function and the self-diffusion constant across a wide range of Fourier time scales. Applying this technique to water measured the intermediate scattering function from $q = 0.01$ to 0.18 Å^{-1} and at Fourier times from 74 to 570 picoseconds. Fitting the data to Eqn. 8 yielded diffusion constants with an average value $2.45 \pm 0.32 \times 10^{-9}$m^2/s, an intermediate point compared to other values reported in the literature.

Like other neutron techniques, there are distinct differences between the application at a constant wavelength source and a time-of-flight source. The ease of tuning the MI-SANS frequency, the simultaneous collection across many MI-SANS times, and the ability to rebin data in the analysis are all distinct advantages of using a time-of-flight source. We envision the time-of-flight MI-SANS technique that we have described here being used on liquids in many sample environments.

6. Acknowledgments

We acknowledge useful discussions with Ad van Well, Dave Baxter and Roger Pynn. This work was partially financed by the Austrian Science Fund (FWF), Projects No. P30677 and P34239. Part of this research was funded by a NWO groot (Grant No. LARMOR 721.012.102). S.J.K. was supported by US Department of Commerce cooperative agreement number 70NANB15H259. We acknowledge the support of Mark Davenport and Emily McFarlane for the ^{3}He cell polarization and installation. *Stephen J. Kuhn and Niels Geerits contributed equally to this work.

References

Amann-Winkel, K., Bellissent-Funel, M., Bove, L.E., Loerting, T., Nilsson, A., Paciaroni, A., Schlesinger, D. & Skinner L., (2016) *Chemical Reviews* **116**,7570-7589

Babcock, E. Salhi, Z. & Ioffe, A (2013). *Journal of the Physical Society of Japan* **82**, SA030-1-10.

Bleuel, M., Littrell, K., Gähler, R., & Lal, J., (2005) *Physica B: Condensed Matter* **365**, 213-217

Bleuel, M., Gähler, R., Lang, E., & Lal, J. (2009) *Nuclear Instruments and Methods in Physics Research A* **600** 220-222

Bleuel, M. & van Well, A. A. (2011) *Physica B Condensed Matter* **406** 2478-2481

Brandl, G., Lai, J, Carpenter J., Crow, L., Robertson, L., Georgii. R., Böni, P., & Bleuel, M., (2012) *Nuclear Instruments and Methods in Physics Research A* **667** 1-4

Boag, S., Parnell, S.R., Frost, C.D., Andersen, K.H., & Babcock, E. (2007) *Physica B: Condensed Matter* **397**, 179-181

Boag, S., Babcock, E., Andersen, K.H., Becker, M., Charlton, T.R., Chen, W.C., Dalgliesh, R.M., Elmore, S.D., Frost, C.D., Gentile, T.R., Lopez Antona, R., Parnell, S.R., Petoukhov, A.K., Skoda, M.W.A., & Soldner, T. (2009) *Physica B: Condensed Matter* **404**, 2659-2662

Cappelletti, R. L.,Udovic, T. J., Li, H., Paul, R. L. (2018) *Journal of Applied Crystallography* **51** 1323-1328

Cavatorta, F., Deriu, A., Di Cola, D., & Middendorf, H. D., (1994) *Journal of Physics Condensed Matter* **6** A113 **A113-A117**

Chen, W.C., Gentile, T.R., Ye, Q., Walker, T.G. & Babcock, E., (2014) *Journal of Applied Physics* **116** 014903-1- 014903-6

Egelstaff, P. A., Haywood, B. C., & Webb, F. J. (1967) *Proceedings of the Physical Society* **90** 681- 696

Farago, B, (2003) *Neutron Spin Echo Spectroscopy: Basics, Trends and Applications* 15-31 pp. 74–86. Berlin, Heidelberg: Springer.

Franz, C., Soltwedel, O., Fuchs, C., Säubert, S., Haslbeck, F., Wendl, A., Jochum, J. K., Böni P., & Pfleiderer, C. (2019) *Nuclear Instruments and Methods in Physics Research A* **939** 22-29

Franz, C. Saubert, S., Wendl, A., Haslbeck, F.X., Soltwedel, O., Jochum, J.K., Spitz, L., Kindervater, J., Bauer, A., Böni, P., & Pfleiderer, C. (2019b) *Journal of the Physical Society of Japan* **88** 081002

Gähler, R. Golub, R. and Keller, T. (1992) *Physica B: Condensed Matter* **180-181** 899 - 902

Geerits, N., Parnell, S.R., Thijs, M.A., van Well, A. A., Franz, C., Washington, A. L., Raspon, D., Dalgliesh, R. M., & Plomp, J. (2019) *Review of Scientific Instruments* **90** 125101-1-125101-7

Golub, R. & Gähler, R. (1987) *Physics Letters A* **123** 43-48

Golub, R. & Lamoreaux, S.K. (1992) *Physics Letters A* **162** 122-128

Hank, P., Besenbock, W., Gähler, R., & Koppe, M. (1997) *Physica B: Condensed Matter* **234**,1130-1132

Holz, M., Heila S.R., and Saccob, A. (2000) *Physical Chemistry Chemical Physics* **2**,4740-4742

Iverson, E.B., Baxter, D.V., Gallmeier, F.X., Gillis, R.C., Hugle, T., Lu, W., McClanahan, T.C., Remec, I., & Rinckel, T.C. (2018) *Journal of Physics: Conference Series* **1021**, 012067

Jochum, J.K., Wendl, A., Keller, T., Franz, C. (2020) *Measurement Science and Technology* **31**, 035902

Keller, T., Golub, R., & Gähler, R. (2002) *Scattering* 1264-1286

Kindervater, J. Martin, N., Häußler, W., Krautloher, M., Fuchs, C.,, Mühlbauer, S., Lim, J.A., Blackburn, E., Böni, P., & Pfleiderer C. (2015) *EPJ Web of Conferences* **83** 03008-p.1-4

Köhli, M., Klein, M., Allmendinger, F. Perrevoort, A-K., T Schröder, T., Martin, N., Schmidt, C. J., and Schmidt, U.(2016) *Journal of Physics: Condensed Matter* **746** 012003

Kruk, D. Meier, R., Haywood, B.C. & Webb, F.J., (2012) *Physical Review E* **85** 020201-1 - 020201-5

Lebedev, V.T., & Torok, D. (1999) *Technical Physics Letters* **25** 116-118

Li, F., Dadisman, R., & Wasilko, D. C. (2020) *Nuclear Instruments and Methods in Physics Research A* **955** 163300

Martin, N., (2018) *Nuclear Instruments and Methods in Physics Research A* **882** 11-16

Mezei, F., (1972) *Zeitscrihft Fur Physik*, **1972** 146-160)

Mezei, F., (2003) *Neutron Spin Echo Spectroscopy: Basics, Trends and Applications* 15-31 pp. 5-14. Berlin, Heidelberg: Springer.

Parnell, S.R. Woolley, E.B., Boag, S. & Frost C.D. (2008) *Measurement Science and Technology* **19** 045601

Parnell, S.R., Babcock, E., Nüninghoff, K., Skoda, M.W.A., Boag, S., Masalovich, S., Chen, W.C., Georgi, R., Wild, J.M. & Frost C.D. (2009) *Nuclear Instruments and Methods in Physics Research A* **598** 774-778

Parnell, S. R., Washington, A. L., Li, K., Yan, H., Stonaha, P., Li, F., Wang, T., Walsh, A., Chen, W.C., Parnell, A.J., Fairclough, J. P. A., Baxter, D. V., Snow, W. M. & Pynn, R. (2015) *Review of Scientific Instruments* **86** 023902-1-10

Price, W.S., (2009) *NMR Studies of Translational Motion*

Qvist, J. Carlos Mattea, C., Sunde, E. P., and Halle, B. (2012) *Journal of Chemical Physics* **136** 204505

Salhi, Z., Babcock, E., Bingöl, K., Bussmann, K., Kammerling, H., Ossovyi, V., Heynen, A., Deng, H., Hutanu, V., Masalovich, S., Voigt, J., & Ioffe, A. (2019) *Journal of Physics: Conference Series* **1316**, 012009-1-8

Teixeira, J., Bellissent-Funel, M.-C., Chen, S. H., & Dianoux, A. J., (1985) *Physical Review A* **31** 1913 -1917

Trappeniers, N. J. Gerritsma, C. J., & Oosting P. H., (1965) *Physics Letters* **18** 256-257

Wiengärtner, H., (1982) *Zeitschrift für Physikalische Chemie* **132** 129-149

Zhao, J., Hamilton, W.A., Lee, S.W., Robertson, J. L., Crow, L., & Kang, Y. W. (2015) *Applied Physics Letters* **107** 113508-1-4

Synopsis

We present a measurement on the self-diffusion of water using the high-resolution neutron scattering technique Modulated intensity - small angle neutron scattering (MI-SANS). This technique uses two tuned RF flippers to create a modulation in the neutron intensity that can resolve dynamics on the picosecond time scale.